Accelerated photosynthesis routine in LPJmL4

Jenny Niebsch[1], Werner von Bloh[2], Kirsten Thonicke[2], and Ronny Ramlau[1]

[1]RICAM, Altenbergerstr. 69, 4040 Linz, Austria

[2]Potsdam Institute for Climate Impact Research (PIK), Member of the Leibniz Association, 14412 Potsdam, Germany

Correspondence: Jenny Niebsch (jenny.niebsch@oeaw.ac.at)

Abstract. The increasing impacts of climate change require strategies for climate adaptation. Dynamic Global Vegetation Models (DGVMs) are one type of multi-sectorial impact models with which the effects of multiple interacting processes in the terrestrial biosphere under climate change can be studied. The complexity of DGVMs is increasing as more and more processes, especially for plant physiology, are implemented. Therefore, there is a growing demand for increasing the computational performance of the underlying algorithms as well as ensuring their numerical accuracy. One way to approach this issue is to analyse the routines which have the potential for improved computational efficiency and/or increased accuracy when applying sophisticated mathematical methods.

In this paper, the Farquhar-Collatz photosynthesis model under water stress as implemented in the Lund-Potsdam-Jena managed Land DGVM (4.0.002) was examined. We additionally tested the uncertainty of most important parameter on photosynthesis as an additional approach to improve model quality. We found that the numerical solution of a nonlinear equation, so far solved with the Bisection method, could be significantly improved by using Newton's method instead. The latter requires the computation of the derivative of the underlying function which is presented. Model simulations show a significant lower number of iterations to solve the equation numerically and an overall run time reduction of the model of about 16 $\%$ depending on the chosen accuracy. Increasing the parameters θ and α_{C3} by 10 $\%$, respectively, while keeping all other parameter at their original value, increased global GPP by 2.384 GtC/yr and 9.542 GtC/yr, respectively. The Farquhar-Collatz photosynthesis model forms the core component in many DGVMs and land-surface models. An update in the numerical solution of the nonlinear equation in connection with adjusting globally important parameter to best known values, can therefore be applied to similar photosynthesis models. Furthermore, this exercise can serve as an example for improving computationally costly routines while improving their mathematical accuracy.

1 Introduction

Climate change is increasingly affecting the world we live in and that in turn affects nature's contribution to our livelihoods, (Pörtner et al., 2022). Estimating the extent and impacts of climate change has become more and more urgent over the last couple of decades. Earth System models as well as impact models are used to develop strategies for climate adaptation and mitigation to achieve the Paris climate accord, (Masson-Delmotte et al., 2021), (Pörtner et al., 2022). Climate change affects vegetation dynamics, biodiversity, water and biogeochemical cycles which could reduce the biosphere's capacity to absorb carbon from the atmosphere in the future. Dynamic Global Vegetation Models (DGVMs) are applied to study the net effects of multiple interacting processes that affect carbon sequestration (photosynthesis) and storage (in biomass and soil), see (Prentice et al., 2007). It shows the demand for reliable and consistent model projections which require continuous work on reducing model uncertainty. While increasing complexity of the models by including more and more processes in DGVMs has been matched by increasing high-performance computing capabilities over the past decades, little has been invested in identifying and optimizing computationally intensive routines in the model (Reichstein et al., 2019). These routines often have a long model history as they frequently belong to the core routines stemming from the very first model version. This includes, e.g., the physiological modelling core of simulating photosynthesis in connection with atmospheric water demand or plant-water stress. The photosynthesis model is based on the Farquhar approach implemented in land-surface schemes of the second generation (Pitman, 2003) followed by first global biome models (Haxeltine and Prentice, 1996a) from which DGVMs evolved later on, (Prentice et al., 2007).

The Farquhar-Collatz approach was implemented in the land surface of the SiB2 model by Sellers et al. (1992, 1996a) where it replaced their empirical photosynthesis model. The photosynthesis model in SiB2 (Sellers et al., 1996b) covers the co-limitation by Rubisco enzyme activity, light availability and export limitation of carbon compounds. Furthermore, it covers the gradient between inner-stomatal CO_2 concentration to the CO_2 concentration around the leaf surface in the computation of stomatal conductance. By implementing the semi-mechanistic photosynthesis model and coupling it to transpiration via stomatal conductance, the LSM could then not only investigate biophysical effects of climate change but also biogeochemical effects of rising atmospheric CO_2 in the Earth System (Pitman, 2003). The SiB2 model (Sellers et al., 1992, 1996a), the NCAR CCM2 model (Bonan et al. , 1995), and the MOSES land surface model of the UK Met office (Cox et al., 1998) were among the first to implement this photosynthesis scheme and evaluated it against field campaigns. At present, the Farquhar-Collatz photosynthesis model is used in a number of Land surface models of the CMIP-5 Earth System Models, such as the Community Atmosphere Biosphere Land Exchange (CABLE) LSM of the Australian Community Climate Earth system Simulator (ACCESS, see (de Kauwe et al., 2015), and ref. therein) as well as the ORCHIDEE DGVM (Krinner et al., 2005) of the IPSL-CM5 Earth System Model (Dufresne et al., 2013). Different models of stomatal conductance were evaluated for the JSBACH LSM (Reick et al., 2013) of the Max Planck Institute Earth System Model (MPI-ESM) to account for hydraulic properties and drought response (Knauer et al., 2015). The Community Land Model CLM4.5 (Oleson et al., 2013) of the NCAR ESM use the Ball-Berry model of stomatal conductance and extended it to account for leaf temperature acclimation and leaf water potential (Bonan et al. , 2014); a similar approach was implemented in the JULES-vn5.6 land surface model (Oliver et al., 2022) of the UK Hadley Centre ESM (Sellar et al., 2019).

While Land surface models detail vertical water, energy and carbon profiles within the canopy, which extrapolates the photosynthetic capacity calculated at the leaf level to canopy photosynthesis (Sellers et al., 1996b), stand-alone DGVMs often use a big-leaf approach and compute daytime photosynthesis for canopy conductance which goes back to the BIOME-3 model (Haxeltine and Prentice, 1996b) which opened up the second line of vegetation models by embedding the Farquhar-Collatz photosynthesis model in a modelling framework of plant physiology and vegetation dynamics in DGVMs (Prentice et al., 2007). The Haxeltine and Prentice (1996b) implementation is used in the LPJ model family originating from Sitch et al. (2003) and the LPJ-GUESS model (Smith et al., 2001, 2014), as well as the current LPJmLv4 model (Schaphoff et al., 2018a, b).

The Farquhar photosynthesis module forms the core of many other DGVMs, see e.g., (Smith et al., 2001, 2014; Krinner et al., 2005). Today, 14 DGVMs (stand-alone and coupled to land-surface models) contribute to the TRENDY intercomparison project (https://blogs.exeter.ac.uk/trendy/) that informs the global carbon project on the state of the land carbon sink (Sitch et al., 2015).

In order to apply the model to the global land surface it is not anymore sufficient to use faster or larger computing infrastructure or try to parallelise the code as in von Bloh et al. (2010). It rather requires the evaluation of the underlying algorithm structure of the code, and in particular the used numerical methods. Replacing 'old' numerical algorithms by modern methods will result in a significantly better run-time performance while simultaneously maintaining or even increasing the accuracy of the method. We quantified the runtime required by each submodule (or routine) of the LPJmL DGVM using the profiling option of the compilation command and the linux gprof utility. We found that the repeated execution of the photosynthesis routine demands a big fraction, i.e. 38%, of the computational time. All other routines require less than 11%.

To illustrate our approach, our goal was to improve the computational efficiency of DGVMs by accelerating the photosynthesis module under water stress conditions using the Lund-Potsdam-Jena DGVM, (Schaphoff et al., 2018a, b), as an example. A key ingredient in the modelling of photosynthesis is the determination of the ratio λ between intracellular and ambient CO_2 concentration. Mathematically, λ is computed as a zero of a nonlinear equation $f(\lambda) = 0$, which has been so far solved by a simple bisection algorithm. We expected to improve the computational efficiency by applying one of the more sophisticated solution methods, namely Regula falsi, secant and Newton's method. In this technical paper, we describe testing all three methods, but found that only with Newton's method the computational efficiency was significantly improved. Only a few, detailed specialized studies mention the use of Newton's or similar methods to solve coupled balance schemes, (Collatz et al. , 1991; Pearcy et al., 1997; Soo-Hyung and Lieth , 2003; Dubois et al., 2007), or extensions of the photosynthesis-transpiration scheme along the leaf-plant-soil continuum in DGVMs (Bonan et al. , 2014) are mentioned, but none provide a documentation on the computational efficiency, or how the numerical method was implemented in the model and/or their code. In addition we test the effect of sensitive photosynthesis parameter on annual GPP of the computationally efficient model where we build on recent work by (Walker et al. , 2020).

We start with a short description of the different mathematical methods to find the zeros of a general nonlinear continuous function f and their advantages and disadvantages. Afterwards we introduce the relevant function f from the photosynthesis module and calculate its derivative. We then compare the performance of Newton's algorithm and bisection in terms of the number of iterations and the computational time that is necessary to achieve a given accuracy. Finally, we benchmark the updated LPJmL version to show that the simulated vegetation dynamics as well as storage and fluxes of carbon and water remain robust.

2 Solution of nonlinear equations

The computation of the ratio λ between intracellular and ambient CO_2 concentration requires to compute the zero of a function $f(\lambda)$. In most cases, this task cannot be solved analytically but requires a numerical approach, mostly based on iterative methods. Given a nonlinear continuous function $f : \mathbb{R} \to \mathbb{R}$, we want to find the zero(s) x_s of this function within a certain interval $[a,b]$. While bisection, regula falsi and secant method are very simple to implement, Newton's method requires the computation of the derivative of f, which will be provided for the photosynthesis equation described in Sub-Section 3.2.

Here, the computational efficiency is determined by the speed of convergence. To compare the methods with respect to the speed of convergence we define the order of convergence: Let x_s be a zero of f found by computing a sequence (x_k) of approximate solutions via an iteration scheme. The iteration method has the order of convergence p if

$$\limsup_{k\to\infty} \frac{\|x_{k+1} - x_s\|}{\|x_k - x_s\|^p} = K \tag{1}$$

with $0 < K < \infty$ and $K < 1$ for $p = 1$. Thus a high order of convergence implies a fast convergence which on the other hand means fewer iteration steps. Numerically, the iteration is stopped either if the function value $f(x_k)$ of the iterate x_k is almost zero, i.e., less than a given accuracy y_{acc}, or if the iterate itself changes less than a given accuracy $|x_k - x_{k-1}| < x_{acc}$.

Let us introduce some of the methods in the following subsections, see Schwarz (2009) for details.

2.1 Bisection

For bisection we have to choose $[a,b]$ such that $f(a) \cdot f(b) < 0$, i.e. $f(a)$ and $f(b)$ have different signs. We compute the midpoint of the interval $x_m = \frac{a+b}{2}$ and its function value $f(x_m)$. If $|f(x_m)| < y_{acc}$ the search is complete, if not we check if $f(a) \cdot f(x_m) < 0$. If the latter is the case, x_s has to be in the interval $[a, x_m]$, otherwise in $[x_m, b]$. We repeat this bisection until either $|f(x_k)| < y_{acc}$ or $|x_k - x_{k-1}| < x_{acc}$. This method always converges but slowly with convergence order $p = 1$, i.e., linear convergence.

2.2 Regula falsi

For the regula falsi method, we also need to choose a, b such that $f(a) \cdot f(b) < 0$. Instead of the midpoint of $[a,b]$ we compute the next iterate x_1 for an approximation of x_s by computing the zero of the linear function through the points $(a|f(a))$ and $(b|f(b))$. Again we check if $|f(x_1)| < y_{acc}$ and abort or check if $f(a) \cdot f(x_1) < 0$ and repeat this procedure either with $[a, x_1]$ or $[x_1, b]$. Convergence is always assured and also linear, i.e., $p = 1$.

2.3 Secant method

The secant method only differs from the regula falsi in that the starting values $a = x_0$ and $b = x_1$ do not have to fulfill the condition $f(a) \cdot f(b) < 0$. The next iterate is computed by

$$x_{k+1} = x_k - f(x_k) \frac{x_k - x_{k-1}}{f(x_k) - f(x_{k-1})}. \tag{2}$$

This method can fail to converge depending on the starting values. If the method converges, it does so with order $p = 1,618$. Since the conditions on the starting values to ensure convergence depend on the knowledge of x_s, in practise a and b still have to fulfill the condition $f(a) \cdot f(b) < 0$.

2.4 Newton's method

Newton's method starts at an arbitrary approximation x_0 of x_s and uses the tangent of the function f at $(x_0, f(x_0))$ to compute the next iterate x_1 as the zero of the tangent. This is repeated, thus the next iterate is always computed from the previous one by

$$x_{k+1} = x_k - \frac{f(x_k)}{f'(x_k)}, \tag{3}$$

provided that $f'(x_k) \neq 0$. The method belongs to the class of fixed point iterations because the computation of the next iterate depends on the previous iterate only. If f is three times differentiable on $[a,b]$ and $f'(x_s) \neq 0$ then there exists an interval $I = [x_s - \delta, x_s + \delta]$ such that f is a contraction on I. It implies that for every start value from I, the method converges at least with order $p = 2$, (Schwarz, 2009). We remark that the gain in convergence speed has to be weighted against the time it takes to compute the derivative of f.

3 Application to the problem

We now analyse the difference in speed of convergence between the bisection and Newton's method when applied to the optimization equation of the photosynthesis routine of the LPJmL DGVM.

3.1 Definition of the function *f*

In presenting the function $f(\lambda)$, we follow the nomenclature of Schaphoff et al. (2018a), which contains a detailed description of the derivation of this function. A list of the used symbols is given in Appendix A. We want to find $\lambda = \frac{c_i}{c_a} = \frac{p_i}{p_a}$, i.e. the ratio between the intracellular and ambient CO_2 concentration, or partial pressure, resp., as the solution of the following equation

$$0 = f(\lambda) \quad = \quad A_{nd}(\lambda) + \left(1 - \frac{dayl}{24}\right) R_{leaf} - \frac{p_a(g_c - g_{min})}{1.6}(1 - \lambda). \tag{4}$$

Here A_{nd} the net daily photosynthesis, R_{leaf} the leaf respiration, $dayl$ the hours of daylight, p_a the ambient partial pressure, g_c the canopy conductance, and g_{min} the minimum canopy conductance for a specific plant functional type (PFT). The first term is the photosynthesis during daylight. It is the gross daily photosynthesis A_{gd} minus leaf respiration, $A_{nd}(\lambda) = A_{gd}(\lambda) - R_{leaf}$. The second term represents the dark respiration, i.e. respiration during night-time. The third term represents the photosynthesis that is possible to achieve a potential canopy conductance. In finding λ such that $f(\lambda) \approx 0$ we actually balance both light- and Rubisco-limited photosynthesis (first two terms) and photosynthesis related to the potential canopy conductance.
To shorten the formulas we define the abbreviation $C_{pg} = \frac{p_a(g_c - g_{min})}{1.6}$:

$$0 = f(\lambda) \quad = \quad A_{gd}(\lambda) - \frac{dayl}{24} R_{leaf} - C_{pg}(1 - \lambda). \tag{5}$$

The second summand does not depend on λ, whereas $A_{gd}(\lambda)$ has a more complex representation. The gross photosynthesis rate A_g is the minimum of the light-limited, J_C, and Rubisco-limited photosynthesis rate, J_E. It can be shown that the minimum can be computed as

$$A_{gd}(\lambda) \quad = \quad \frac{dayl}{2\theta}\left[J_E(\lambda)+J_C(\lambda)-\sqrt{(J_E(\lambda)+J_C(\lambda))^2-4\theta J_E(\lambda)J_C(\lambda)}\right] \tag{6}$$

where θ is a shape parameter that allows for a gradual transition from one limitation to the other. Light-limited photosynthesis depends on the absorbed photosythetically active radiation $APAR$, Rubisco-limited photosynthesis is determined by the maximum Rubisco capacity V_m:

$$J_E(\lambda) \quad = \quad C_1(\lambda)\frac{APAR}{dayl}, \tag{7}$$

$$J_C(\lambda) \quad = \quad C_2(\lambda)V_m. \tag{8}$$

Setting the internal partial pressure $p_i = \lambda p_a$ and using another abbreviation $C_K := K_c(1+\frac{[O_2]}{K_O})$, where K_c is the Michaelis constant for CO_2, $[O_2]$ and K_O are the partial pressure and the Michaelis constant for oxigen, we have

$$C_1(\lambda) \quad = \quad \begin{cases} T_{stress}\ \alpha_{C3}\ \frac{\lambda p_a-\Gamma_*}{\lambda p_a+(2)\Gamma_*} & \text{for C3- Photosynthesis} \\ T_{stress}\ \alpha_{C4}\ \frac{\lambda}{\lambda_{maxC4}} & \text{for C4- Photosynthesis} \end{cases} \tag{9}$$

$$C_2(\lambda) \quad = \quad \begin{cases} \frac{\lambda p_a-\Gamma_*}{\lambda p_a+C_K} & \text{for C3- Photosynthesis} \\ 1 & \text{for C4- Photosynthesis.} \end{cases} \tag{10}$$

Here, α_{C3} and α_{C4} are the intrinsic quantum efficiencies for CO_2 uptake in C_3 and C_4 plants, resp. Γ_* is the carbone dioxide compensation point and T_{stress} is a temperature stress function defined as

$$T_{stress} = \frac{1-0.01e^{T_3(T_d-T_4)}}{1+e^{T_1(T_2-T_d)}} \tag{11}$$

with T_d as the daily air temperature and T_1 to T_4 being PFT-specific temperature parameters, (Sitch et al., 2000). LPJmL simulates vegetation dynamics for the 10 PFTs; we provide the parameter values used for T_1 to T_4 in Appendix A, table A2, for the PFT types from Schaphoff et al. (2018a).

3.2 Derivative of *f*

To compute the derivative f' of f we rearrange (5):

$$f(\lambda) = A_{gd}(\lambda) + C_{pg}\lambda - C_{pg} - \frac{dayl}{24}R_{leaf} \tag{12}$$

Since the last two terms are constant the derivative is given by

$$f'(\lambda) \quad = \quad A'_{gd}(\lambda) + C_{pg}. \tag{13}$$

To determine A'_{gd} we apply sum, chain, and product rule of differentiation to (6) and get

$$A'_{gd}(\lambda) \quad = \quad \frac{dayl}{2\theta}\left[J'_E + J'_C - \frac{[J_E+J_C][J'_E+J'_C]-2\theta[J'_EJ_C+J_EJ'_C]}{\sqrt{(J_E+J_C)^2-4\theta J_EJ_C}}\right]. \tag{14}$$

The derivatives of J_E and J_C are given by

$$J'_E(\lambda) = C'_1(\lambda)\frac{APAR}{dayl}, \tag{15}$$

$$J'_C(\lambda) = C'_2(\lambda)V_m. \tag{16}$$

To compute C'_1 from (9) and C'_2 from (10) we use the quotient rule

$$C'_1(\lambda) = \begin{cases} T_{stress}\ \alpha_{C3}\ \frac{2(3)p_a\Gamma_*}{(\lambda p_a+(2)\Gamma_*)^2} & \text{for } C_3\text{- Photosynthesis} \\ \frac{T_{stress}\ \alpha_{C4}}{\lambda_{max_{C4}}} & \text{for } C_4\text{- Photosynthesis} \end{cases} \tag{17}$$

$$C'_2(\lambda) = \begin{cases} \frac{p_a(C_K+\Gamma_*)}{(\lambda p_a+C_K)^2} & \text{for } C_3\text{- Photosynthesis} \\ 0 & \text{for } C_4\text{- Photosynthesis.} \end{cases} \tag{18}$$

We describe the consequent changes in the model code which were required to implement the computation of the derivative *fcnd*(λ) in the Appendix B.

The function f is defined for all $\lambda > 0$, as long as $(J_E(\lambda) + J_C(\lambda))^2 \geq 4\theta J_E(\lambda)J_C(\lambda)$. As a composition of at least three times differentiable functions it fulfills the differentiability condition of Newton's method. The parameters in the definition of f vary with the geographic location and season. A plot of f for parameters from different locations (boreal, temperate, and tropical) and at different times can be seen in Figure 1.

The condition $f'(\lambda) \neq 0$ as well as the suitability of a staring value can not be generally ensured. In all our computations convergence was not a problem. To be on the safe side, one can implement a hybrid method that switches to bisection if convergence of the iterates does not occur.

4 Numerical performance and discussion

We have tested the different methods in the routine regarding computational time and number of iterations for given accuracy x_{acc}. There was no significant speed-up with the secant and regula falsi method. Hence, we concentrated on the comparison of Bisection and Newton's method and describe the outcome in this section.

In a first test, the LPJmL model was run over 120 simulation years and the number of iterations in the Bisection and Newton's routine was counted and averaged over all grid cells and one year (Figure 2). For $x_{acc} = 0.01$ this number was about 3 for Newton's method and 7 for Bisection (dotted lines in Figure 2). When x_{acc} was set to 0.001 the number of iterations with Newton's method increased only slightly whereas the Bisection method needed 9 to 10 iterations (solid lines in Figure 2). Until now, the bisection algorithm used 10 as the maximal number of iterations. Using maximum 10 iterations fits to the interval width of $2^{-10} \approx 0.001$, our accuracy measure x_{acc}. Increasing the maximum number of iterations had no effect on the number of required iterations. We conclude that Newton's method reduces the necessary number of iteration to a third.

In a next step, a spin-up run of LPJmL over 5000 simulation years was conducted to compare the time performance using both routines. Usually, LPJmL simulation experiments start from bare ground, i.e. initial vegetation conditions are not prescribed.

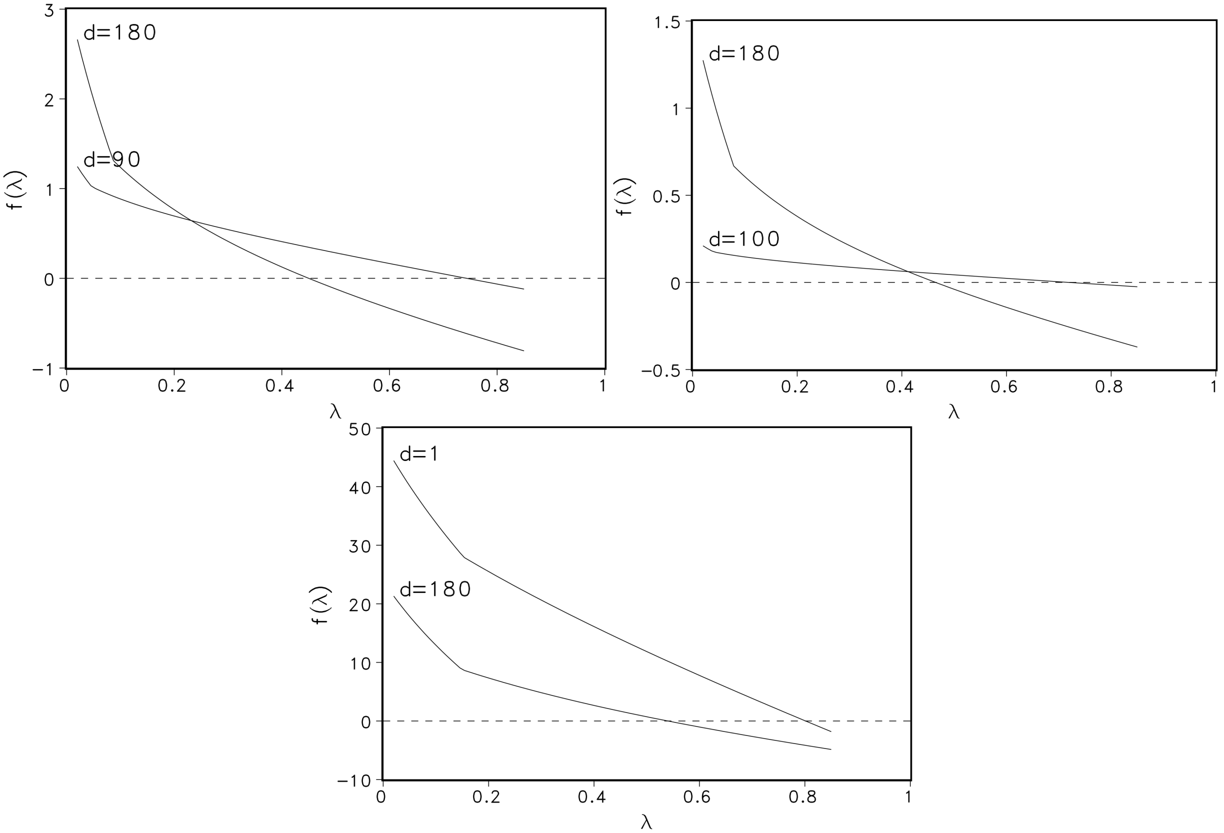

Figure 1. Function $f(\lambda)$ for a set of parameters from different days in 1901 and locations, namely Hainich (Germany, mixed-temperate forest; upper left), Seiteminen (Finland, boreal forest; upper right) and Santarem (Brazil, tropical rainforest; lower). d denotes the day in year 1901.

Therefore, a spin-up run is used to bring all vegetation and soil carbon pools into equilibrium with climate. For the usually implemented accuracy $x_{acc} = 0.1$ the computation time for 5000 years was about 5250 s in both cases. This means that the advantage of Newton's method in terms of iteration numbers is levelled by the additional time for computing the derivative of f. For $x_{acc} = 0.01$, the Bisection method needed 6700 s, while Newton's method 5600 s. Thus a reduction of about 16% in time could be observed. It implies that with almost the same amount of time (5250 s vs. 5600 s) a higher accuracy can be achieved with Newton's method (Figure 3). While the accuracy y_{acc} does not increase significantly for the Bisection method for $x_{acc} = 0.001$, we gain 2 orders of magnitude increase in y_{acc} for the Newton's method. As a result, a change of x_{acc} from 0.1 to 0.01 will be permanently implemented in the LPJmL model for future model applications. We expect that with the implementation of new model developments that affect the photosynthesis module (e.g., nutrient limitation from nitrogen and leaf temperatures) an efficient and increased model accuracy (y_{acc}) for finding the zero of $f(\lambda)$ will be even more important. It can be expected that the computation time for the Bisection method would increase substantially, while increasing only moderately for Newton's method.

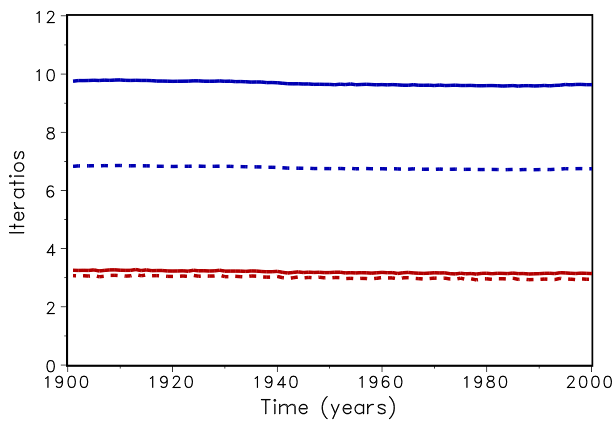

Figure 2. Average number of iteration for Bisection (upper lines, blue) and Newton (lower lines, red) for accuracy $x_{acc} = 0.01$ (dotted) and 0.001 (solid)

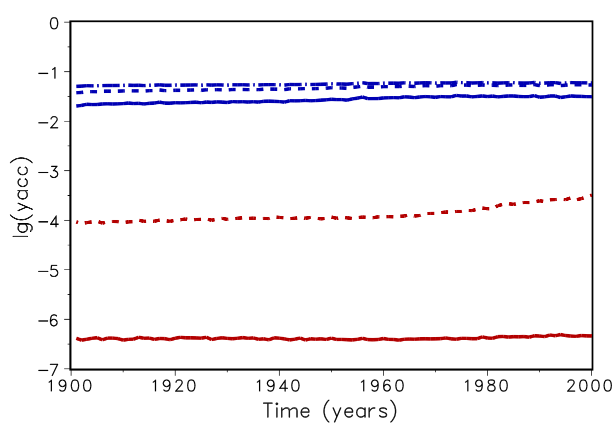

Figure 3. Mean decadic logarithm of the accuracy y_{acc} for Bisection (upper lines, blue) and Newton (lower lines, red) for accuracy $x_{acc} = 0.01$ (dotted) and 0.001 (solid). The dashed-dotted line shows the accuracy of the original version of LPJmL.

In order to check if the implementation of Newton's method is robust for all important model variables, we performed a transient simulation with the LPJmL model starting from the spin-up and covering the years 1901-2000. Model configuration and input data are as in Schaphoff et al. (2018a). We compared the main diagnostic variables of the published LPJmL4.0 version against the version using the Newton's Method (see Appendix C). We found that most global diagnostic variables related to fluxes and storage of carbon and water had differences of $< \pm 1.0\%$, including total vegetated area. Only marginal changes (+3 gC per mA^2 and month) in net primary productivity (NPP), heterotrophic respiration and evaporation are seen mainly in

Europe and southern as well as southeastern Asia. The reductions in carbon storage in litter and soil are very small and apply only to the boreal zone across the northern hemisphere and central Europe (compare spatial maps of carbon and water variables in Appendix C).

The photosynthesis module is also applied to the crop functional types and managed grassland within LPJmL4.0. Therefore, sawing dates, crop productivity and harvest are among the simulated variables. Comparing both model versions in the model benchmark, we found that global harvest changed for a number of crops. Rainfed and irrigated rice increased by 5% and 8%, respectively, mainly in India and southeast Asia. Harvest of rainfed temperate cereals increased by $< 1.0\%$, mainly found in central Europe. Harvest of irrigated temperate cereals (incl. wheat) increased by 4.5%, which mainly applied to India as well. Harvest of irrigated and rainfed soybean increased by 2.3% and 1.5% globally, the differences are mainly found in the US and Brazil. All other crop functional types had marginal to zero changes in global productivity as well as simulated harvest (see Table in Appendix C).

For all global carbon pools (vegetation and soil) and carbon (GPP, heterotrophic respiration and fire emissions) as well as water fluxes (transpiration and runoff) we found no difference in the temporal changes in the transient simulation over the 20th century. All variables showed similar, if not identical dynamics (data not shown). Small changes were found in the fractional coverage of plant functional types, i.e. most differences were negligible. The fractional coverage of Temperate broadleaved summergreen trees increased by 4.8% globally, which mainly applies to Europe, northeastern US and parts of China. Increases in temperate C_3 grasses are found in the boreal zone, summing up to 4.8% globally. Marginal changes of $< 0.5\%$ per grid cell are found for all other PFTs which imply small adjustments in vegetation composition in these vegetation zones (see difference maps in Appendix C). Comparisons using flux tower measurements on carbon and water fluxes as well as discharge data showed no differences so that we can conclude that also for these variables the results are robust (data not shown). We can therefore conclude that the LPJmL results were robust before, but are now achieved due to improved accuracy of the photosynthesis routine.

After improving the computational efficiency and numerical precision, we can now test the parameter uncertainties following Walker et al. (2020), who tested the sensitivity of $\theta, \alpha_{C3}, b_{C3}, k_{c25}, K_{o25}$ on their impacts on global GPP. The LPJmL model computes V_m as follows Schaphoff et al. (2018a), eq. (35):

$$V_m = \frac{1}{b_{C3}} \cdot \frac{c_1}{c_2} \cdot ((2\theta - 1) * s - (2\theta * s - c_2) * \sigma) \cdot APAR. \tag{19}$$

Therefore, the sensitivity of V_{cmax} results from varying b_{C3} indirectly since the reciprocal of b_{C3} is used to calculate V_{cmax} in a linear equation. Varying b_{C3} is therefore the adequate sensitivity test which relates to V_{cmax}. We varied each parameter by 10% independently and find that θ ($\alpha_{C3}, b_{C3}, k_{c25}, K_{o25}$) increases global annual GPP (AGPP, hereafter) by 1.67% (+6.69%, -1.67%, -0.35%, +0.14%). Table 1 shows the difference of the two most important parameter on global AGPP.

parameter	Δ GPP relative in %	Δ GPP absolute (GtC/yr)
θ	1.67	2.384
α_{C3}	6.68	9.542
b_{C3}	-0.56	-0.798
k_{c25}	-0.35	-0.506
K_{o25}	0.14	0.199

Table 1.

Change in the AGPP after varying the listed parameters by 10%. GPP is calculated as the global average mean for the years 1901-2000.

Geographically, increasing θ yields higher AGPP mainly in the tropics and temperate forest regions, where AGPP increases up to 100 gC/m^2. However, AGPP increases between 200 and 500 gC/m^2 when changing α_{C3}, see Fig.4. It turns out that AGPP is increased in all regions, where LPJmL simulates woody PFTs. Also here, largest effects are seen in (sub-)tropical and temperate regions which span larger areas than the areas with increased AGPP as a result of varying θ.

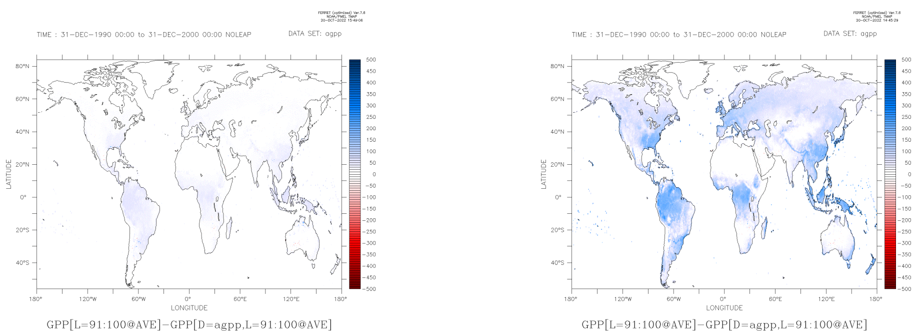

Figure 4. Parameter sensitivity on Annual Gross Primary Productivity (AGPP, average of 1901-2000) shown as difference between new parameter and reference simulation. Both simulations have the Newton approach implemented. Increasing θ by 10 % increased AGPP mainly in forested regions (left panel). Increasing α_{C3} by 10 % has a much larger effect on AGPP, especially in the tropics (right panel).

We remark that future work on the photosynthesis approach could focus on the new Johnson and Berry scheme (Johnson and Berry , 2021) with the advantage of calculating gas-exchange and relying less on empirical coefficients.

5 Conclusions

The computational load of Dynamic Global Vegetation Models, caused by increased complexity of the modelling processes, has been so far counteracted by the used high performance computing systems. However, more recently it has become clear that updates in computing infrastructure are not sufficient anymore. Consequently, we proposed to carefully evaluate the algorithmic structure of DGVMs and identify and update routines that can benefit from the use of modern mathematical methods. As a showcase, we investigated the photosynthesis model in the LPJmL DGVM. Specifically, we investigated the computation of the ratio λ between intracellular and ambient CO_2, which is obtained as the zero of a function f. We proposed to replace the so far used bisection method by a Newton method, which is known to converge significantly faster. We carefully compared the model performance of the published LPJmL4.0 version with the version developed in this study and found that the model performance is robust. Using a more sophisticated mathematical method in the photosynthesis module allowed for a higher precision in the computation of λ and resulted in slightly increased productivity in continental and mountainous areas. We think that the new results are more accurate than the previous version due to the higher accuracy of the Newton method visible in Figure 3. With the currently implemented accuracy bounds, the run-time of the model with the Newton routine implemented is about 16$\%$ lower than the old version. This advantage will be much more prominent if the complexity of the model is further extended or if more accurate modelling results are required. Consequently, the Newton based routine will be implemented in the LPJmL model. Additionally we believe that the Newton method can also be applied to photosynthesis modules in other DGVMs and increase model accuracy and/or computational efficiency.

Code and data availability. The model code is available at https://doi.org/10.5281/zenodo.6644541 .

Appendix A: Parameters in photosynthesis

A_{nd}	daily net photosynthesis
dayl	day length
R_{leaf}	leaf respiration
p_a	ambient partial pressure
g_c	canopy conductance
g_{min}	PFT-specific minimum canopy conductance
A_{gd}	daily gross photosynthesis
θ	co-limitation (shape) parameter
J_E	light limited photosynthesis rate
J_C	Rubisco limited photosynthesis rate
APAR	absorbed photosynthetically active radiation
V_m	maximum Rubisco capacity
K_C	Michaelis constant for CO_2
$[O_2]$	O_2 partial pressure
K_O	Michaelis constant for O_2
T_{stress}	Temperature stress function limiting photosynthesis at low and high temperatures
α_{C3}	intrinsic quantum efficiencies for CO_2 uptake in C_3 plants
α_{C4}	intrinsic quantum efficiencies for CO_2 uptake in C_4 plants
Γ_*	carbone dioxide compensation point
λ_{maxC4}	maximum ratio of intracellular to ambient CO_2 for C_4-photosynthesis

Table A1.

General parameters used in the photosynthesis routine. PFT - Plant functional type

Plant Functional Type (PFT)	T_1	T_2	T_3	T_4
Tropical broadleaved evergreen tree	2.0	25.0	30.0	55.0
Tropical broadleaved raingreen tree	2.0	25.0	30.0	55.0
Temperate needleleaved evergreen tree	-4.0	20.0	30.0	42.0
Temperate broadleaved evergreen tree	-4.0	20.0	30.0	42.0
Temperate broad-leaved summergreen tree	-4.0	20.0	25.0	38.0
Boreal needle-leaved evergreen tree	-4.0	15.0	25.0	38.0
Boreal needle-leaved summergreen tree	-4.0	15.0	25.0	38.0
Polar C_3 grass	-4.0	10.0	30.0	45.0
Temperate C_3 grass	-4.0	10.0	30.0	45.0
Tropical C_4 grass	6.0	20.0	45.0	55.0

Table A2.

PFT-specific parameter for temperature stress function (eq.12) in °C. PFT types as in Schaphoff et al. (2018a)

Appendix B: Programming

To implement Newton's method in the LPJmL code, changes had to be made in the functions `photosynthesis.c`, `gp_sum.c` and `water_stressed.c`. (separate file)

New function `newton.c`: see source code in a separate file.

Remark

The function `photosynthesis.c` within LPJmL computes the value $A_{nd}(\lambda) + \left(1 - \frac{dayl}{24}\right) R_{leaf}$ for a given λ. In the function `water_stressed.c` the function `fcn`(λ) is defined as $fcn(\lambda) = C_{pg} * (1-\lambda) - photosythesis(lambda)$, i.e. $fcn = -f$. In order to use Newton's Method we have to compute not only *fcn*(λ) but also its derivative $fcnd(\lambda) = -f'(\lambda)$.

Appendix C: Benchmark results

LPJmL Benchmark

Actual vegetation

Author: Werner von Bloh

Date: 27.04.2022

Benchmark run: newton_e3/output/

Run: bisect_e3/output/

Description: LPJ Benchmark 2022-04-27

Global sums: Veg. incl. LU 1991-2000

Parameter	Lit. estimates	Bm. Run	Run	Diff. abs.	Diff %
Vegetation carbon [GtC]	460 - 660 (1, 2, 3)	595.9	596.2	0.231	0.039
Total soil carbon density [GtC]	2376 - 2456 (4), 1567 (5), 1395 (6)	1862	1862	-0.08	-0.004
Litter carbon [GtC]	NA	151.3	151.4	0.116	0.077
Fire carbon emission [GtC/year]	2.14 (1.6 Nat.Fire) (7, 8, 9, 10)	3.108	3.109	0.001	0.036
Establishment flux [GtC/year]	NA	0.161	0.161	0	-0.002
Area All natural vegetation [M ha]	NA	7767	7767	-0.119	-0.002
Area Tropical broadleaved evergreen tree [M ha]	NA	1180	1179	-0.237	-0.02
Area Tropical broadleaved raingreen tree [M ha]	NA	1280	1280	0.448	0.035
Area Temperate needleleaved evergreen tree [M ha]	NA	364	360.8	-3.166	-0.87
Area Temperate broadleaved evergreen tree [M ha]	NA	322	321.5	-0.467	-0.145
Area Temperate broadleaved summergreen tree [M ha]	NA	136	142.5	6.517	4.792
Area Boreal needleleaved evergreen tree [M ha]	NA	429.2	426.8	-2.393	-0.558
Area Boreal broadleaved summergreen tree [M ha]	NA	916.8	919.6	2.814	0.307

Parameter	Lit. estimates	Bm. Run	Run	Diff. abs.	Diff %
Area Boreal needleleaved summergreen tree [M ha]	NA	378.3	380.7	2.398	0.634
Area Tropical c4 grass [M ha]	NA	893.2	890.6	-2.573	-0.288
Area Temperate c3 grass [M ha]	NA	535.7	545.2	9.472	1.768
Area Polar c3 grass [M ha]	NA	1332	1320	-12.93	-0.971
NPP [GtC/year]	66.05 (11), 62.6 (2), 49.52 - 59.74 (12)	62.81	62.87	0.064	0.102
Heterotrophic respiration [GtC/year]	NA	50.78	50.83	0.044	0.086
Evaporation [10.. km3/year]	NA	9.644	9.661	0.017	0.173
Transpiration [10.. km3/year]	NA	47.83	47.82	-0.011	-0.024
Interception [10.. km3/year]	NA	7.914	7.912	-0.002	-0.024
Runoff [10.. km3/year]	NA	54.3	54.23	-0.064	-0.118
Harvested carbon rainfed tece [Mt DM/year]	524.08 (13)	458.5	462.6	4.106	0.895
Harvested carbon rainfed rice [Mt DM/year]	492.66 (13)	125.2	131.5	6.304	5.035
Harvested carbon rainfed maize [Mt DM/year]	498.33 (13)	434.9	434.8	-0.07	-0.016
Harvested carbon rainfed soybean [Mt DM/year]	NA	126.3	128.1	1.87	1.481
Harvested carbon irrigated tece [Mt DM/year]	524.08 (13)	156.7	163.7	7.038	4.493
Harvested carbon irrigated rice [Mt DM/year]	492.66 (13)	206.4	223	16.64	8.062
Harvested carbon irrigated maize [Mt DM/year]	498.33 (13)	153.1	153.1	-0.002	-0.001
Harvested carbon irrigated soybean [Mt DM/year]	NA	12.03	12.3	0.268	2.229
tree cover fraction [-]	NA	0.644	0.645	0.001	0.12

(1) Olson et al. 1985, (2) Saugier et al. 2001, (3) WBGU 1998, (4) Batjes et al. 1996, (5) Eswaran et al. 1993, (6) Post et al. 1982, (7) Seiler & Crutzen 1980, (8) Andreae & Merlet 2001, (9) Ito & Penner 2004, (10) van der Werf et al. 2004, (11) Vitousek et al. 1986, (12) Ramakrishna et al. 2003, (13) FAOSTAT 1990-2000

Table D1. Global numbers for benchmark with bisection and newton method

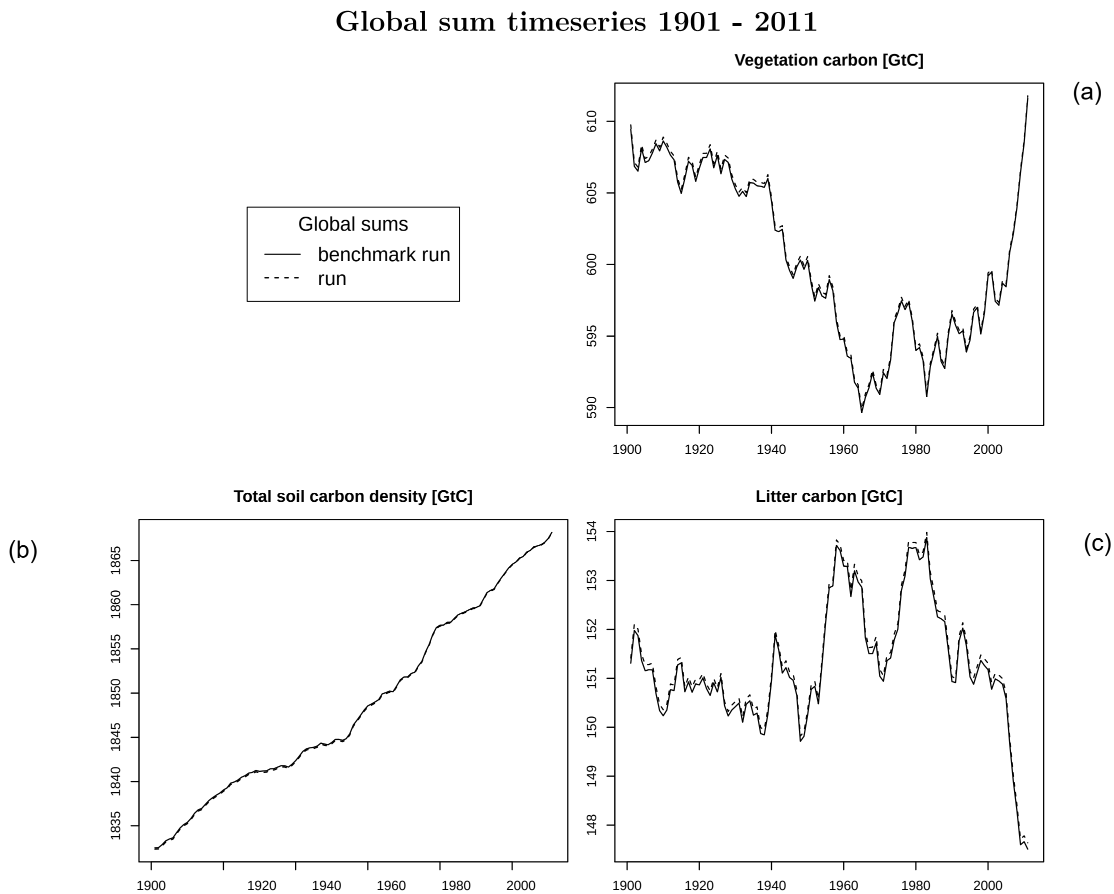

Figure D1. Global numbers for (a) vegetation carbon, (b) total soil carbon,(c) litter carbon

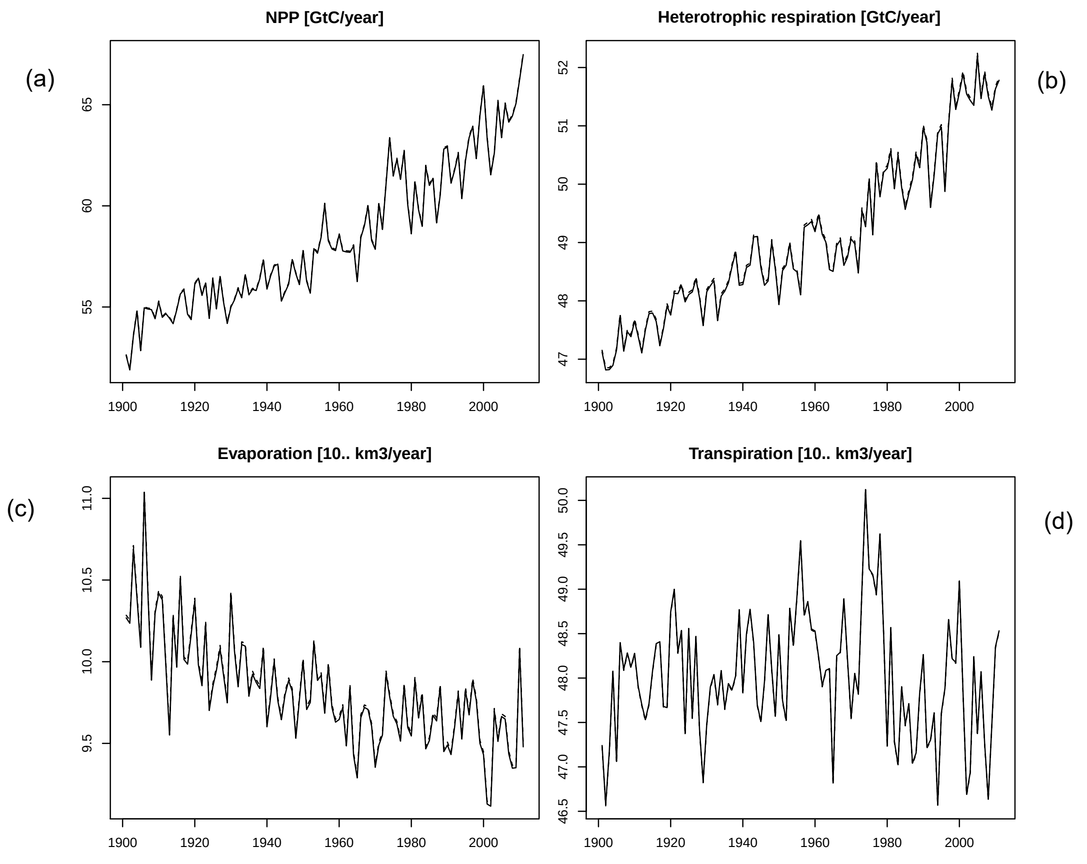

Figure D2. Global sum for time series of (a) NPP, (b) heterotrophic respiration, (c) evaporation, (d) transpiration.

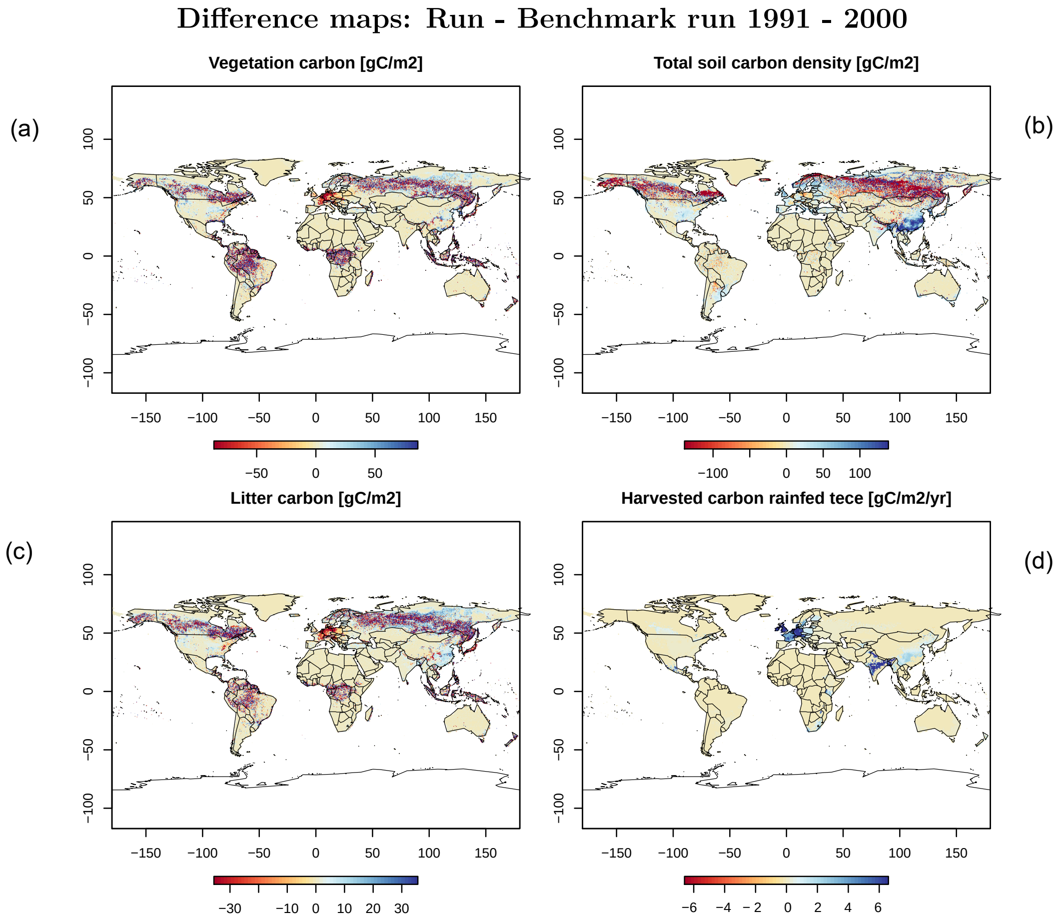

Figure D3. Difference maps of (a) vegetation carbon, (b) soil carbon, (c) litter carbon, (d) harvested carbon of rainfed temperate cereals (tece).

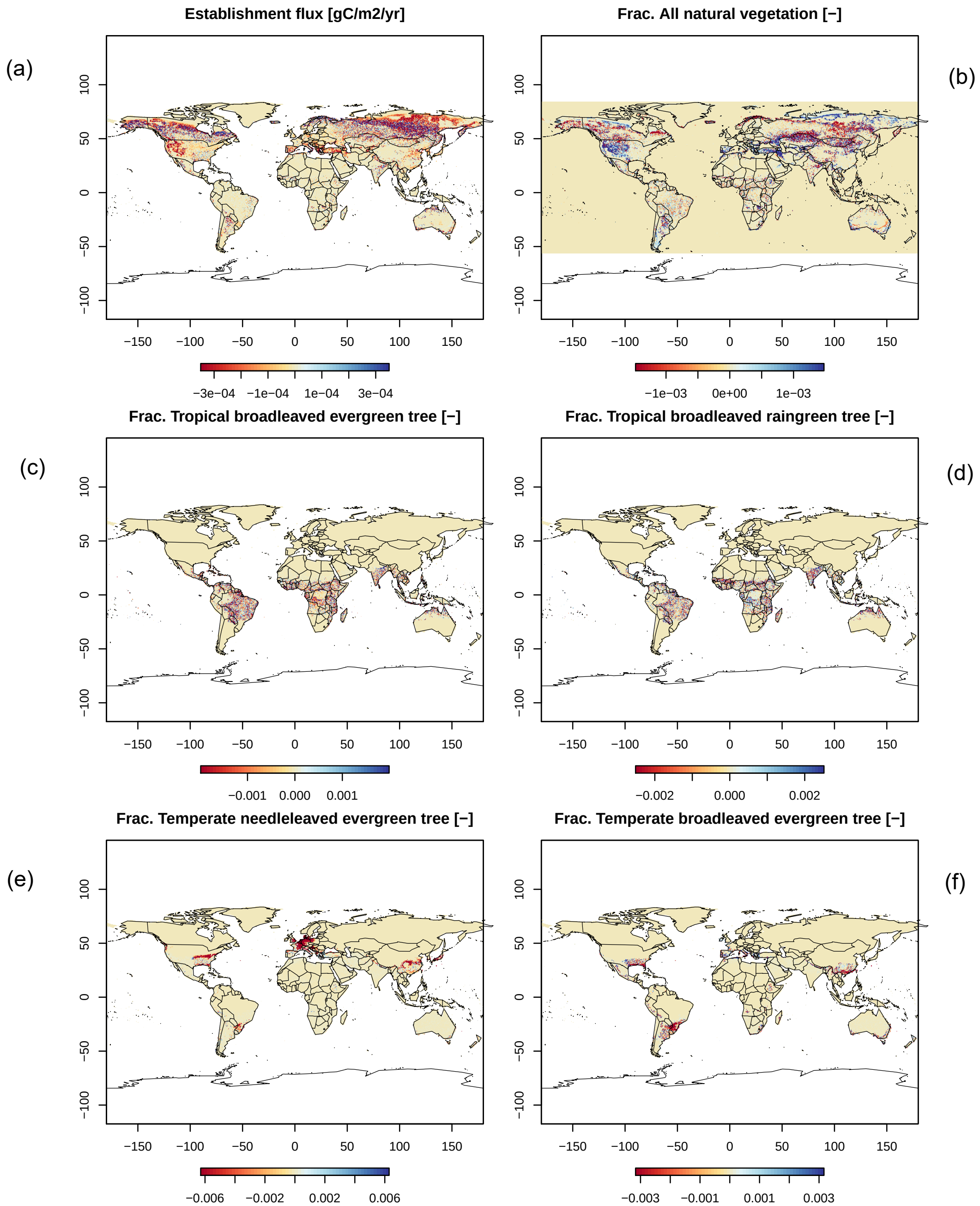

Figure D4. Difference maps of (a) establishment, (b) all natural vegetation, (c) frac. tropical broadleaved evergreen, (d) frac. tropical broadleaved raingreen, (e) frac. temperate needleleaved evergreen, (f) frac. temperate broadleaved evergreen.

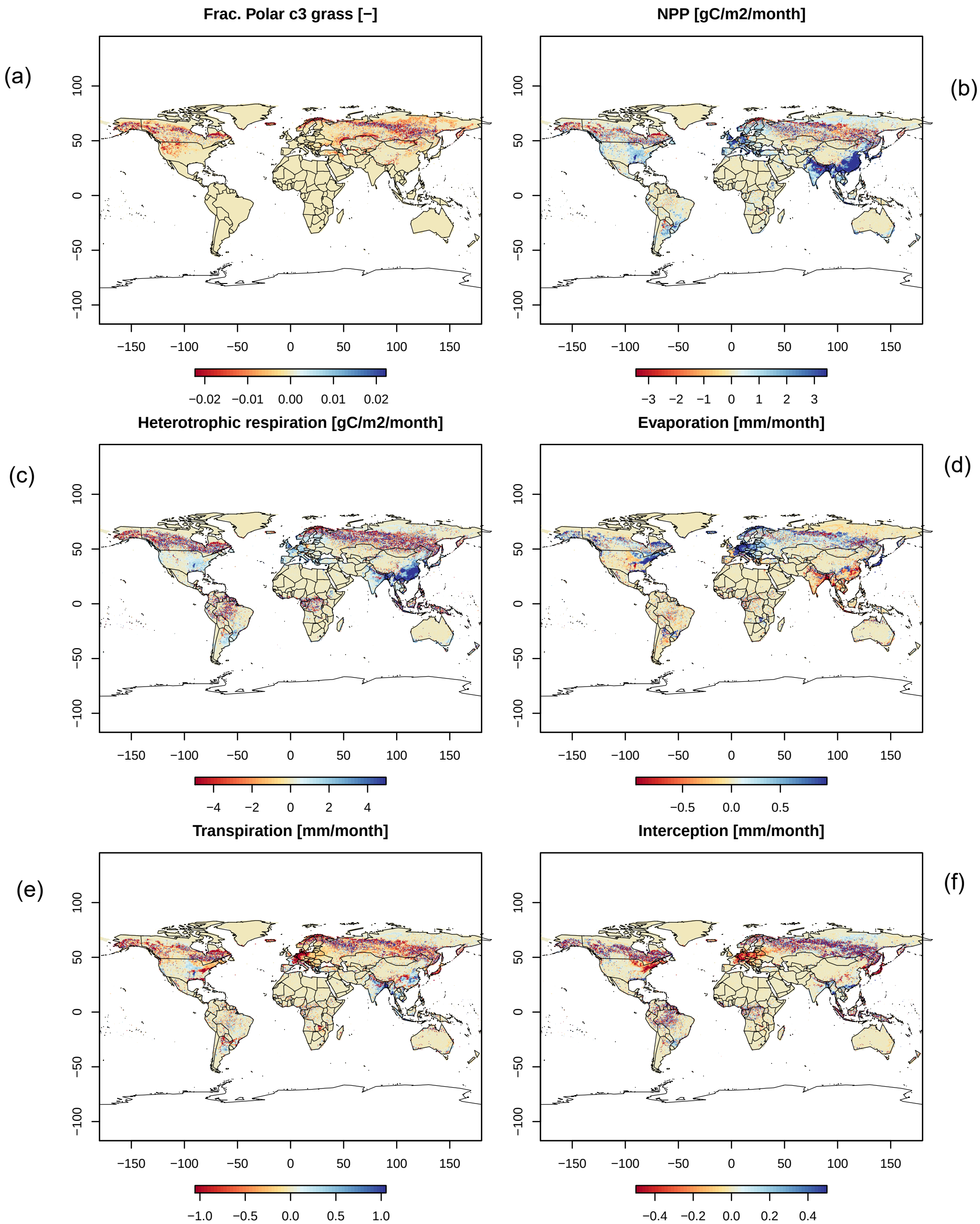

Figure D5. Difference maps of (a) frac. polar C3 grass, (b) NPP, (c) heterotrophic respiration, (d) evaporation, (e) transpiration, (f) interception.

(a)

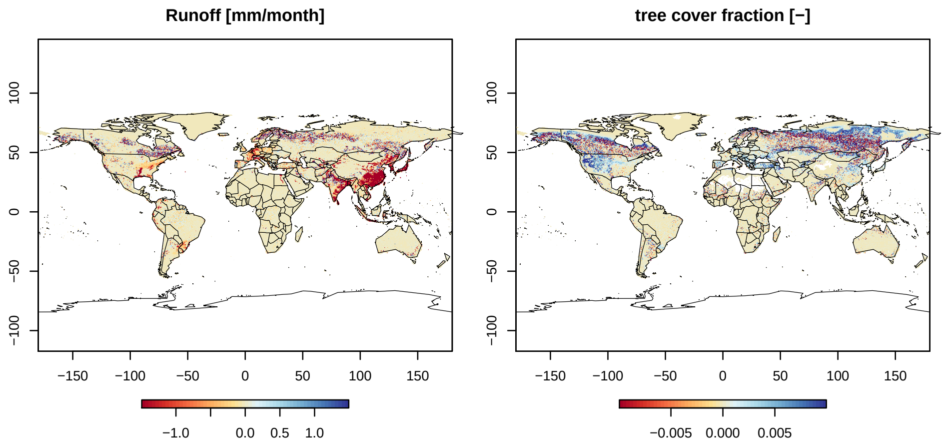

(b)

Figure D6. Difference maps of (a) runoff and (b) tree cover fraction.

Author contributions. JN and RR performed the mathematical analysis, JN and WvB implemented and tested the new numerical methods, WvB conducted the simulation experiments and analysed the model performance and computation efficiency. JN and KT wrote the paper, all authors contributed to the writing of the paper and discussion of the model study throughout to develop the work.

Competing interests. There are no competing interests.

Acknowledgements. The authors gratefully acknowledge the European Regional Development Fund (ERDF), the German Federal Ministry of Education and Research, and the Land Brandenburg for supporting this project by providing resources on the high-performance computer system at the Potsdam Institute for Climate Impact Research. We thank Marie Hemmen from PIK for her support in benchmarking the LPJmL model.

References

Bonan, G.B.: Land–atmosphere CO2 exchange simulated by a land surface process model coupled to an atmospheric general circulation model. Journal of Geophysical Research, 100, 2817–2831, 1995.

Bonan, G. B., Williams, M., Fisher, R. A., and Oleson, K. W.: Modeling stomatal conductance in the earth system: linking leaf water-use efficiency and water transport along the soil–plant–atmosphere continuum, Geosci. Model Dev., 7, 2193–2222, https://doi.org/10.5194/gmd-7-2193-2014, 2014.

Collatz, G.J., Ball, J.T., Grivet, C. and Berry, J.A.: Physiological and environmental regulation of stomatal conductance, photosynthesis and transpiration: a model that includes a laminar boundary layer. Agric. For. Meteorol,, 54: 107-136, https://doi.org/10.1016/0168-1923(91)90002-8, 1991.

Collatz G.J., Ribas-Carbo M., Berry J.A.: Coupled Photosynthesis-Stomatal Conductance Model for Leaves of C4 Plants. Functional Plant Biology 19, 519-538, https://doi.org/10.1071/PP9920519, 1992.

Cox P.M., Huntingford C., and Harding R.J.: A canopy conductance and photosynthesis model for use in a GCM land surface scheme. Journal of Hydrology 212–213, 79–94, 1998.

De Kauwe, M. G., Kala, J., Lin, Y.-S., Pitman, A. J., Medlyn, B. E., Duursma, R. A., Abramowitz, G., Wang, Y.-P., and Miralles, D. G.: A test of an optimal stomatal conductance scheme within the CABLE land surface model, Geosci. Model Dev., 8, 431–452, https://doi.org/10.5194/gmd-8-431-2015, 2015.

Dubois, J.-J.B., Fiscus, E.L., Booker, F.L., Flowers, M.D. and Reid, C.D.: Optimizing the statistical estimation of the parameters of the Farquhar–von Caemmerer–Berry model of photosynthesis. New Phytologist, 176, 402-414, https://doi.org/10.1111/j.1469-8137.2007.02182.x, 2007

Dufresne, J.L., Foujols, M.A., and Denvil, S. et al.: Climate change projections using the IPSL-CM5 Earth System Model: from CMIP3 to CMIP5. Clim Dyn 40, 2123–2165, https://doi.org/10.1007/s00382-012-1636-1, 2013.

Farquhar, G. D., von Caemmerer, S., and Berry, J. A.: A biochemical model of photosynthetic CO2 assimilation in leaves of C3 species. Planta, 149(1), 78–90, https://doi.org/10.1007/BF003 86231, 1980.

Haxeltine, A., and Prentice, I. C.: BIOME3: An equilibrium terrestrial biosphere model based on ecophysiological constraints, resource availability, and competition among plant functional types, Global Biogeochemical Cycles, 10, 693-709, https://doi.org/10.1029/96GB023441996, 1996.

Haxeltine, A., and Prentice, I. C.: A general model for the light-use efficiency of primary production, Functional Ecology, 10, 551-561, https://doi.org/10.2307/2390165, 1996.

Johnson, J.E. and Berry, J.A.: The role of cytochrome b6f in the control of steady- state photosynthesis: a conceptual and quantitative model, Photosynthesis Research, 148(3), pp.101-136, 2021

Knauer, J., Werner, C., and Zaehle, S.: Evaluating stomatal models and their atmospheric drought response in a land surface scheme: A multibiome analysis, J. Geophys. Res. Biogeosci., 120, 1894– 1911, doi:10.1002/2015JG003114, 2015.

Krinner, G., Viovy, N., Noblet-Ducoudré, N. d., Ogée, J., Polcher, J., Friedlingstein, P., Ciais, P., Sitch, S., and Prentice, I. C.: A dynamic global vegetation model for studies of the coupled atmosphere-biosphere system, Global Biogeochemical Cycles, 19, https://doi.org/10.1029/2003GB002199, 2005.

Masson-Delmotte, V., Zhai, P., Pirani, A., Connors, S.L., Péan, C., Berger, S., Caud, N., Chen, Y., Goldfarb, L., Gomis, M.I., Huang, M., Leitzell, K., Lonnoy, E., Matthews, J.B.R., Maycock, T.K., Waterfield, T., Yelekçi, O., Yu, R., and Zhou, B., (eds.) IPCC, 2021: Summary for Policymakers. In: Climate Change 2021: The Physical Science Basis. Contribution of Working Group I to the Sixth Assessment Report of the Intergovernmental Panel on Climate Change, Cambridge University Press. In Press. https://doi.org/10.1017/9781009157896.

Oleson, K. W., Lawrence, D. M., Bonan, G. B., Drewniak, B., Huang, M., Koven, C. D., Levis, S., Li, F., Riley, W. J., Subin, Z. M., Swenson, S. C., Thornton, P. E., Bozbiyik, A., Fisher, R., Heald, C. L., Kluzek, E., Lamarque, J.-F., Lawrence, P. J., Leung, L. R., Lipscomb, W., Muszala, S., Ricciuto, D. M., Sacks, W., Sun, Y., Tang, J., and Yang, Z.-L.: Technical description of version 4.5 of the Community Land Model (CLM), NCAR Tech. Note NCAR/TN-503+STR, National Center for Atmospheric Research, Boulder, Colorado, 420 pp., 2013.

Oliver, R. J., Mercado, L. M., Clark, D. B., Huntingford, C., Taylor, C. M., Vidale, P. L., McGuire, P. C., Todt, M., Folwell, S., Shamsudheen Semeena, V., and Medlyn, B. E.: Improved representation of plant physiology in the JULES-vn5.6 land surface model: photosynthesis, stomatal conductance and thermal acclimation, Geosci. Model Dev., 15, 5567–5592, https://doi.org/10.5194/gmd-15-5567-2022, 2022.

O'Neill, B. C., Tebaldi, C., van Vuuren, D. P., Eyring, V., Friedlingstein, P., Hurtt, G., Knutti, R., Kriegler, E., Lamarque, J.-F., Lowe, J., Meehl, G. A., Moss, R., Riahi, K., and Sanderson, B. M.: The Scenario Model Intercomparison Project (ScenarioMIP) for CMIP6, Geoscientific Model Development, 9, 3461–3482, https://doi.org/10.5194/gmd-9-3461-2016, 2016.

Pearcy, R.W., Gross, L.J. and HE, D.: An improved dynamic model of photosynthesis for estimation of carbon gain in sunfleck light regimes. Plant, Cell and Environment, 20: 411-424. https://doi.org/10.1046/j.1365-3040.1997.d01-88.x, 1997.

Pitman, A.J.: The evolution of, and revolution in, land surface schemes designed for climate models. Int. J. Climatol., 23, 479-510, https://doi.org/10.1002/joc.893, 2003.

Pörtner, H.-O., Roberts, D.C., Poloczanska, E.S., Mintenbeck, K., Tignor, M., Alegria, A., Craig, M., Langsdorf, S., Löschke, S., Möller, V., Okem, A. (eds.) IPCC, 2022: Summary for Policymakers In: Climate Change 2022: Impacts, Adaptation, and Vulnerability. Contribution of Working Group II to the Sixth Assessment Report of the Intergovernmental Panel on Climate Change, Cambridge University Press. In Press.

Prentice, I. C., Bondeau, A., Cramer, W., Harrison, S. P., Hickler, T., Lucht, W., Sitch, S., Smith, B., and Sykes, M. T.: Dynamic global vegetation modelling: quantifying terrestrial ecosystem responses to large-scale environmental change. In: Canadell, J.G., Pataki, D. E., and Pitelka L. F. (Eds.),Terrestrial Ecosystems in a Changing World, Springer, Springer Nature, https://doi.org/10.1007/978-3-540-32730-1, 2007.

Reichstein, M., Camps-Valls, G., Stevens, B., Jung, M., Denzler, J., Carvalhais, N., and Prabhat: Deep learning and process understanding for data-driven Earth system science, Nature, 566, 195-204, https://doi.org/10.1038/s41586-019-0912-1, 2019.

Reick, C., Raddatz, T., Brovkin, V., and Gayler, V.: Representation of natural and anthropogenic land cover change in MPI-ESM, J. Adv. Model. Earth Syst., 5, 459–482, doi:10.1002/jame.20022, 2013.

Schaphoff, S., von Bloh, W., Rammig, A., Thonicke, K., Biemans, H., Forkel, M., Gerten, D., Heinke, J., Jägermeyr, J., Knauer, J., Langerwisch, F., Lucht, W., Müller, C., Rolinski, S., and Waha, K.: LPJmL4 - a dynamic global vegetation model with managed land, Part 1: Model description, Geoscientific Model Development, 11, 1343-1375, https://doi.org/10.5194/gmd-11-1377-2018, 2018.

Schaphoff, S., Forkel, M., Müller, C., Knauer, J., von Bloh, W., Gerten, D., Jägermeyr, J., Lucht, W., Rammig, A., Thonicke, K., and Waha, K.: LPJmL4 - A dynamic global vegetation model with managed land, Part 2: Model evaluation, Geoscientific Model Development, 11, 1377-1403, https://doi.org/10.5194/gmd-11-1377-2018, 2018.

Schwarz, H. R., Köckler, N.: Numerische Mathematik, Ed.7, Vieweg+Teubner, Wiesbaden, https://doi.org/10.1007/978-3-8348-9282-9, 2009.

Sellar, A. A., Jones, C. G., Mulcahy, J. P., Tang, Y., Yool, A., Wiltshire, A., O'Connor, F. M., Stringer, M., Hill, R., Palmieri, J., Woodward, S., de Mora, L., Kuhlbrodt, T., Rumbold, S. T., Kelley, D. I., Ellis, R., Johnson, C. E., Walton, J., Abraham, N. L., Andrews, M. B., Andrews, T., Archibald, A. T., Berthou, S., Burke, E., Blockley, E., Carslaw, K., Dalvi, M., Edwards, J., Folberth, G. A., Gedney, N., Griffiths, P. T., Harper, A. B., Hendry, M. A., Hewitt, A. J., Johnson, B., Jones, A., Jones, C. D., Keeble, J., Liddicoat, S., Morgenstern, O., Parker, R. J., Predoi, V., Robertson, E., Siahaan, A., Smith, R. S., Swaminathan, R., Woodhouse, M. T., Zeng, G., and Zerroukat, M.: UKESM1: Description and Evaluation of the U.K. Earth System Model, J. Adv. Model. Earth Sy., 11, 4513–4558, https://doi.org/10.1029/2019MS001739, 2019.

Sellers, P.J., Berry, J.A., Collatz, G.J., Field, C.B., and Hall, F.G.: Canopy reflectance, photosynthesis, and transpiration. III. A reanalysis using improved leaf models and a new canopy integration scheme, Remote sensing of environment, 42(3), pp.187-216, https://doi.org/10.1016/0034-4257(92)90102-P, 1992.

Sellers, P.J., Randall, D.A., Collatz, G.J., Berry, J.A., Field, C.B., Dazlich, D.A., Zhang, C., Collelo, G.D., and Bounoua, L.: A revised land surface parameterization (SiB2) for atmospheric GCMs. Part I: Model formulation, Journal of climate, 9(4), pp.676-705,https://doi.org/10.1175/1520-0442(1996)009<0676:ARLSPF>2.0.CO;2, 1996.

Sellers, P.J., Tucker, C.J., Collatz, G.J., Los, S.O., Justice, C.O., Dazlich, D.A., and Randall, D.A.: A revised land surface parameterization (SiB2) for atmospheric GCMs. Part II: The generation of global fields of terrestrial biophysical parameters from satellite data. Journal of climate, 9(4), pp.706-737, https://doi.org/10.1175/1520-0442(1996)009<0706:ARLSPF>2.0.CO;2, 1996.

Sitch, S., Prentice, I. C., Smith, B., Cramer, W., Kaplan, J., Lucht, W., Sykes, M., Thonicke, K., and Venevsky, S.: LPJ- a coupled model of vegetation dynamics and the terrestrial carbon cycle, Doctoral dissertation, Institute of Plant Ecology, Lund University, Lund, 213 pp., https://doi.org/10.5194/BG-11-2027-2014, 2000.

Sitch, S., Smith, B., Prentice, I. C., Arneth, A., Bondeau, A., Cramer, W., Kaplan, J. O., Levis, S., Lucht, W., Sykes, M. T., Thonicke, K., Venevsky, S.: Evaluation of ecosystem dynamics, plant geography and terrestrial carbon cycling in the LPJ dynamic global vegetation model, Global Change Biology, 9, 161-185, 10.1046/j.1365-2486.2003.00569.x, 2003

Sitch, S., Friedlingstein, P., Gruber, N., Jones, S. D., Murray-Tortarolo, G., Ahlström, A., Doney, S. C., Graven, H., Heinze, C., Huntingford, C., Levis, S., Levy, P. E., Lomas, M., Poulter, B., Viovy, N., Zaehle, S., Zeng, N., Arneth, A., Bonan, G., Bopp, L., Canadell, J. G., Chevallier, F., Ciais, P., Ellis, R., Gloor, M., Peylin, P., Piao, S. L., Le Quéré, C., Smith, B., Zhu, Z., and Myneni, R.: Recent trends and drivers of regional sources and sinks of carbon dioxide, Biogeosciences, 12, 653–679, https://doi.org/10.5194/bg-12-653-2015, 2015

Smith, B., Prentice, I. C., and Sykes, M.: Representation of vegetation dynamics in modelling terrestrial ecosystems: comparison two contrasting approaches within European climate space, Global Ecology and Biogeography, https://doi.org/10.1046/j.1466-822X.2001.t01-1-00256.x, 2001.

Smith, B., Wårlind, D., Arneth, A., Hickler, T., Leadley, P., Siltberg, J., and Zaehle, S.: Implications of incorporating N cycling and N limitations on primary production in an individual-based dynamic vegetation model, Biogeosciences, 11, 2027-2054, https://doi.org/10.5194/bg-11-2027-2014, 2014.

Soo-Hyung, K., Lieth, J.H.: A Coupled Model of Photosynthesis, Stomatal Conductance and Transpiration for a Rose Leaf (Rosa hybrida L.), Annals of Botany, Volume 91(7), 771–781, https://doi.org/10.1093/aob/mcg080, 2003

von Bloh, W., Rost, S., Gerten, D., and Lucht, W.: Efficient parallelization of a dynamic global vegetation model with river routing, Environmental Modelling & Software, 25, 685-690, https://doi.org/10.1016/j.envsoft.2009.11.012, 2010.

Walker, A.P., Johnson, A.L., Rogers, A., Anderson, J., Bridges, R.A., Fisher, R.A., Lu, D., Ricciuto, D.M., Serbin, S.P., and Ye, M: Multi-hypothesis comparison of Farquhar and Collatz photosynthesis models reveals the unexpected influence of empirical assumptions at leaf and global scales. Glob Change Biol. 2021; 27: 804– 822. https://doi.org/10.1111/gcb.15366, 2020.